This article has been accepted for publication in a future issue of this journal, but has not been fully edited. Content may change prior to final publication. Citation information: DOI 10.1109/TIE.2020.2965430, IEEE Transactions on Industrial Electronics

Active Common Mode Voltage-Based Open-Switch Fault Diagnosis of Inverters in IM Drive Systems

Yitao Cheng, Yao Sun, *Member, IEEE*, Xing Li, Hanbing Dan, *Member, IEEE*, Jianheng Lin and Mei Su, *Member, IEEE*

***Abstract*—Fast and reliable fault diagnosis is essential for induction motor (IM) drive systems with high reliability requirements. This paper proposes a robust open-switch fault diagnosis method based on the common mode voltages of the inverter in IM drive systems. This method makes full use of the characteristics of common mode voltages: 1) the calculated common mode voltages (CCMVs) are equal to each other under normal operating conditions and the CCMVs represent the other behaviors under fault conditions; 2) average common mode voltage is a degree of freedom in the modulation of the inverter. Based on the first characteristics, the CCMVs are used to detect and locate the open-switch faults of the inverters. Based on the second one, an active common mode voltage injection (ACMVI) method is proposed to improve the credibility of the diagnosis results and reduce the rate of missed detection. The proposed diagnosis algorithm only uses the measured current information, avoiding the application of extra sensors. And its average detection time is about 300us, which is three switching cycles. Simulation and experimental results are presented to demonstrate the feasibility and effectiveness of the proposed fault diagnosis method.**

***Index Terms*—Calculated common mode voltages, active common mode voltage injection, fault diagnosis, open-switch faults, voltage source inverter (VSI), induction motor (IM).**

I. Introduction

Nowadays, voltage source inverters (VSIs) have been widely used in motor drive systems and micro-grid systems. However, electrical faults of the VSI pose a threat to the safe operation of these systems [1]-[3]. Therefore, the fast and reliable fault diagnosis becomes important to improve the system reliability and avoid harmful accidents. It has been reported that 38% of the electrical faults in the ac drive systems are power circuit faults [4]-[5]. And most of them are semiconductor device faults, such as open-switch and short-circuit faults. In recent years, the open-switch faults have received much attention and numerous methods have been proposed to detect and isolate these faults in the inverters [6]-[7]. These methods can be classified into two categories by the measured variables: current-based [8]-[18] and voltage-based methods [19]-[31].

In current-based methods, the average current methods, the slope methods and the current observer-based methods are the most commonly used ones. In addition, wavelet packet transform is also suggested to detect the inverter faults in [18]. The average current methods [8]-[12] detect the open-switch faults from the mean value of output currents. In [8], Mendes uses the average value of currents in the complex plane αβ to detect open-switch faults, applying Park vector method. However, it has a drawback of load dependence. To make the fault diagnosis algorithm independent of load, Diallo proposed an approach based on the Concordia stator mean current vector in [9]. However, these methods are not suitable for the closed-loop control schemes. Thus, Estima [10] proposes an improved scheme based on the errors of the normalized currents average absolute values. It is independent of the system control scheme and has immunity to false alarms. In [11], the normalized phase currents and current zero-cross detection methods are used simultaneously to reduce the effect of current distortion. In the slope methods [13]-[14], the slope of the current space vector trajectory is used to detect the faults, which is assumed to be constant for a quarter of current period. And to locate the fault switches, Schmitt Triggers are used to detect the polarity of the currents during the faults. Previous methods utilize the measured currents to detect the open-switch faults, and the detection time usually takes a fundamental period. The current observer-based method [15]-[17] can effectively reduce the detection time. A current residual vector-based method is proposed in [15]. This approach uses the current residual between the estimated value and measured value to detect the faults. It gets rid of the effects of the load and control strategy and reduces the detection time to a quarter of fundamental wave period. [16] proposed a faster detection method based on the observation of the current control deviation and an additional voltage test procedure. It can detect the open-switch faults within a few switching periods, even during transient operation.

Manuscript received June 11, 2019; revised September 1, 2019, October 30, 2019 and December 9, 2019; accepted December 9, 2019. This work was supported in part by the National Key R&D Program of China under Grant 2018YFB0606005, the National Natural Science Foundation of China under Grant 61622311, the Project of Innovation-driven Plan in Central South University under Grant 2019CX003, the Major Project of Changzhutan Self-dependent Innovation Demonstration Area under Grant 2018XK2002. (*Corresponding author: Yao Sun.*)

Yitao Cheng, Yao Sun, Hanbing Dan, Jianheng Lin and Mei Su are with the School of Automation, Central South University and the Hunan Provincial Key Laboratory of Power Electronics Equipment and Gird, Changsha 410083, China (E-mail: csuxtt@gmail.com; yaosuncsu@gmail.com; daniel698@sina.com; mltortoise@163.com; sumeicsu@csu.edu.cn).

Xing Li is with the College of Electrical and Information Engineering Hunan University, Changsha 410082, China (E-mail: lxhnu@hnu.edu.cn).

This article has been accepted for publication in a future issue of this journal, but has not been fully edited. Content may change prior to final publication. Citation information: DOI 10.1109/TIE.2020.2965430, IEEE Transactions on Industrial Electronics

Compared with the current-based methods, many early voltage-based approaches usually need extra voltage sensors. [19] proposed four detection techniques based on an analytical model of the VSI, which are achieved by comparing the key points' measurement voltages with their references. It needs multiple voltage sensors and the detection time is one fourth of the fundamental cycle. In [20], a fast fault diagnosis method based on the line-to-line voltage measurement is proposed, which is applied in VSI-fed IM drive systems. It uses two voltage sensors and can detect the single and multiple open-switch faults. For open-phase faults, a method based on zero-sequence voltage components (ZSVC) is proposed in [21], and it can discriminate the fault types, such as internal stator winding failure and switches failure. For shorter detection time, [22] and [23] develop a field-programmable gate array (FPGA)-based fault diagnosis approach. This method can detect the faults within less than 10 us. [24] proposed a faster fault detection method for insulated-gate bipolar transistors (IGBTs), which can reduce the detection time to less than 3 us. However, the shorter detection time will result in higher system cost. In order to balance the system cost and detection time, [25] proposed an open-circuit fault diagnosis method using two voltage transformers. This method detects the faults by comparing the preprocessed diagnosis eigenvalue with the output voltage envelope, and the open-switch faults can be located in one carrier period.

To avoid the extra voltage measurements, [26] proposed a fault diagnosis algorithm for the inverters in micro-grids, which is based on the analysis of the waveform features and composition for the main fault component. However, its detection time is long. To reduce the detection time, some fault diagnosis approaches [27]-[29] based on model predictive control (MPC) are proposed, which can detect the open-switch faults within several switching cycles. In [27], its fault diagnosis method is based on the error voltage. It estimates the actual line-to-line voltages from the system analysis model. And the residuals between the reference and the estimated value are used to detect and locate the fault switches. However, these methods are both highly dependent on the model parameters, which reduces the robustness of the diagnosis system. [30] proposed an open-circuit diagnosis approach in closed-loop PWM ac regenerative drives, which is insensitive to model parameter errors. In addition, the artificial intelligence method [31] is also suggested to detect the faults in the H-bridge multilevel inverters. It can ignore the effect of the system nonlinear factors. However, it requires complex calculation which is not easy to achieve in actual controllers.

In this paper, a fast and reliable open-switch fault diagnosis technique based on the calculated common mode voltages (CCMVs) is proposed. And the main contributions are listed below:

1) No additional hardware is needed, avoiding extra costs;

2) Common mode voltage is used for fault diagnosis, providing new thinking for the related researchers;

3) Active common mode voltage injection method and robust differentiator are proposed in this paper, which can improve the reliability of fault diagnosis, reduce the rate of false alarms and increase the robustness of the algorithm.

In the method, two different thresholds are designed as double insurance to detect and locate the single and multiple open-switch faults. The first threshold is relatively small, which is sensitive to all the exceptional cases. It is mainly used as the trigger condition for the active common mode voltage injection (ACMVI) method. The other threshold is used as the final decision conditions for the faults. If a real open-switch fault occurs, the residuals will exceed the first threshold. Then the ACMVI method will be triggered. And it actively enlarges the residuals and makes them exceed the second threshold. As a result, the open-switch fault is detected. If the residuals caused by noises and parameter variations exceed the first threshold, the residuals will not be enlarged by the ACMVI method. Then, the false alarm can be avoided. Therefore, the proposed fault diagnosis method is robust, which can effectively reduce the rate of missed detection and false alarm.

This paper is organized as follows. In Section II, the simplified model of the system and the fundamental principle of the proposed method are analyzed. In Section III, the fault-diagnosis strategy is described in detail. And the simulation and experimental results are introduced and analyzed in Section IV, V. In Section VI, we give the conclusion.

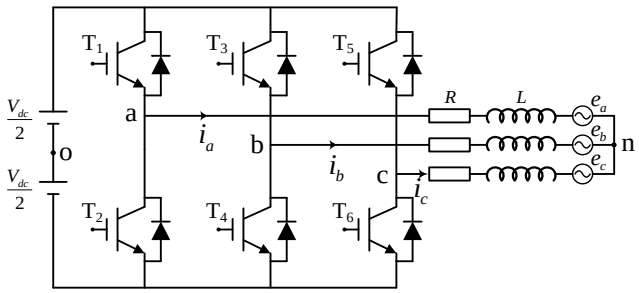

Fig. 1. Simplified model of VSI-Based IM system.

II. Fundamental Principle of Calculated Common Mode Voltage-Based Fault Diagnosis

A. Modeling of VSI-based IM System

The simplified equivalent circuit of the VSI-based induction motor (IM) system is illustrated in Fig. 1, where the IM is equivalent to a series RL circuit with a back electromotive force (EMF). In fact, the equivalent circuit can also represent other cases such as VSI-based PMSM and VSI-based grid-connected systems.

From Fig.1, the switching average model of the converter is expressed as follows:

$$\begin{cases} u_{no} = u_{ao} - Ri_a - L\dfrac{di_a}{dt} - e_a \\ u_{no} = u_{bo} - Ri_b - L\dfrac{di_b}{dt} - e_b \\ u_{no} = u_{co} - Ri_c - L\dfrac{di_c}{dt} - e_c \end{cases} \tag{1}$$

This article has been accepted for publication in a future issue of this journal, but has not been fully edited. Content may change prior to final publication. Citation information: DOI 10.1109/TIE.2020.2965430, IEEE Transactions on Industrial Electronics

where u_{ao}, u_{bo} and u_{co} are the average output phase voltages, and u_{no} is the average common mode voltage. i_a, i_b and i_c are the stator currents. e_a, e_b and e_c are the back EMFs. R is the stator resistance, and L is the stator leakage inductance.

In normal operation, u_{no} is equal to its reference value u_{no}^* which is called zero-sequence signal in carrier-based modulation.

B. Basic Principle of Proposed Method

Based on (1), the concepts of CCMVs are defined as follows:

$$\begin{cases} u_{no\_a}=u_{ao}^*-Ri_a-L\dfrac{di_a}{dt}-e_a \\ u_{no\_b}=u_{bo}^*-Ri_b-L\dfrac{di_b}{dt}-e_b \\ u_{no\_c}=u_{co}^*-Ri_c-L\dfrac{di_c}{dt}-e_c \end{cases} \tag{2}$$

where u_{ao}^*, u_{bo}^* and u_{co}^* are the references of u_{ao}, u_{bo} and u_{co}.

In the normal operation, the CCMVs will satisfy the following relation:

$$u_{no\_a}=u_{no\_b}=u_{no\_c} \tag{3}$$

TABLE I
THE CCMVS UNDER DIFFERENT FAULT CONDITIONS

Single Open-switch Faults	Fault switch	Multiple Open-switch Faults	Fault switch
$u_{no\_a}=u_{no\_b}=u_{no\_c}$	–	①&&②	T_1,T_2
		①&&③	T_1,T_3
		①&&④	T_1,T_4
$u_{no\_a}>u_{no\_b}$, $u_{no\_b}=u_{no\_c}$ $\Rightarrow$ ①	T_1	①&&⑤	T_1,T_5
		①&&⑥	T_1,T_6
$u_{no\_a}<u_{no\_b}$, $u_{no\_b}=u_{no\_c}$ $\Rightarrow$ ②	T_2	②&&③	T_2,T_3
		②&&④	T_2,T_4
$u_{no\_b}>u_{no\_a}$, $u_{no\_a}=u_{no\_c}$ $\Rightarrow$ ③	T_3	②&&⑤	T_2,T_5
		②&&⑥	T_2,T_6
$u_{no\_b}<u_{no\_a}$, $u_{no\_a}=u_{no\_c}$ $\Rightarrow$ ④	T_4	③&&④	T_3,T_4
		③&&⑤	T_3,T_5
$u_{no\_c}>u_{no\_a}$, $u_{no\_a}=u_{no\_b}$ $\Rightarrow$ ⑤	T_5	③&&⑥	T_3,T_6
		④&&⑤	T_4,T_5
$u_{no\_c}<u_{no\_a}$, $u_{no\_a}=u_{no\_b}$ $\Rightarrow$ ⑥	T_6	④&&⑥	T_4,T_6
		⑤&&⑥	T_5,T_6

In the case of an open-switch fault, there exists a phase i where $u_{io}^*\neq u_{io}$ and $i\in\{a,b,c\}$, then (3) no longer holds. For example, assuming that switch T_1 suffers an open-switch fault and $i_a>0$, then the actual output voltage u_{ao} is equal to $-u_{dc}/2$ and less than its reference u_{ao}^*. According to (2), the CCMVs will satisfy the following relation:

$$u_{no\_a}>u_{no\_b}=u_{no\_c} \tag{4}$$

If other single open-switch faults happen, similar analysis could be conducted. All the fault diagnosis results are summarized in Table I. ①~⑥ represent the CCMV conditions corresponding to six different single-open-switch faults. If the multiple open-switch faults happen, they could be identified from the combinations of ①~⑥.

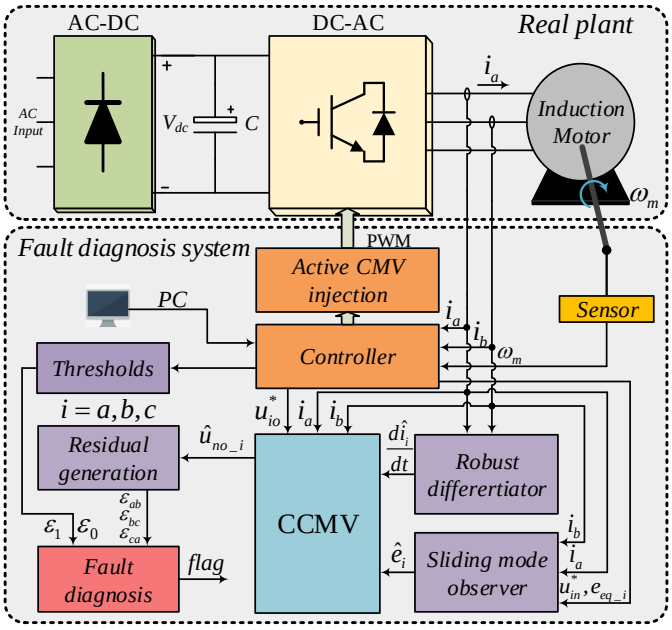

Fig. 2. The proposed overall control and fault-diagnosis block diagram.

III. FAULT-DIAGNOSIS STRATEGY

A. Overall Control and Fault-Diagnosis Block Diagram

Based on the analysis before, the CCMVs information could be used for open-switch fault diagnosis. However, in actual application, it is not easy to obtain the CCMVs accurately. The reasons are summarized as follows:

1) The back EMFs in (2) cannot be measured directly, it should be estimated;

2) From (2), the derivative operator will be involved to obtain the CCMVs, which is sensitive to noises.

3) The estimation of the EMFs depends on model parameters.

To overcome the difficulties mentioned above, a robust differentiator is introduced to calculate the derivative of currents. A sliding mode observer is proposed to estimate the unknown back EMFs. And an active common mode voltage injection idea is presented to improve the robustness of fault diagnosis. The proposed overall control and fault-diagnosis block diagram are shown in Fig. 2.

B. Robust Differentiator for Currents

[32] proposed a practical first-order robust differentiator which can alleviate the influence of possible measurement noises. In this paper, it is used to obtain the derivative parts of the load currents. The equations are as follows:

$$\begin{cases} \dot{x}=u \\ u=u_1-\lambda\left|x-f(t)\right|^{1/2}sign(x-f(t)) \\ \dot{u}_1=-\alpha sign(x-f(t)) \end{cases} \tag{5}$$

where x is the observed current, $f(t)$ is the sampling current, u is

This article has been accepted for publication in a future issue of this journal, but has not been fully edited. Content may change prior to final publication. Citation information: DOI 10.1109/TIE.2020.2965430, IEEE Transactions on Industrial Electronics

the output of the differentiator. In practice, a low-pass filter with a high cut-off frequency is used to smooth the output of the differentiator. To ensure that the dynamic error of the observer converges to zero, the parameters α, λ should satisfy the following sufficient conditions:

$$\alpha > m > 0, \quad \lambda^2 \geq 4m\frac{\alpha + m}{\alpha - m} \tag{6}$$

where *m* is the Lipschitz's constant of the signal *f(t)*. Condition (6) only results from a very crude estimation. Therefore, the specific values of α, λ need to be adjusted in practical applications.

C. Sliding Mode Observer for Back EMFs

The dynamic equations of IM with back EMF in the stationary reference frame are as follows:

$$\begin{cases} L_\sigma \dfrac{di_a}{dt} = u_{an}^* - R_s i_a - e_a \\ L_\sigma \dfrac{di_b}{dt} = u_{bn}^* - R_s i_b - e_b \\ L_\sigma \dfrac{di_c}{dt} = u_{cn}^* - R_s i_c - e_c \\ \dfrac{L_m}{L_r}\dfrac{d\psi_{ri}}{dt} = e_i, i \in (a,b,c) \end{cases} \tag{7}$$

where $L_\sigma = \sigma L_s$ and $\sigma = 1 - L_m^2/(L_s L_r)$ are the leakage inductance and leakage coefficient; i_i , ψ_{ri} and e_i are the stator currents, rotor flux and back EMF; u_{in}^* are stator reference voltages before the third harmonic injection; R_s is stator resistance; R_r is rotor resistance; L_m is magnetizing inductance; L_s is stator inductance; L_r is rotor inductance.

Based on (7), three sliding mode observers are designed to obtain e_i :

$$\begin{cases} L_\sigma \dfrac{d\hat{i}_i}{dt} = u_{in}^* - R_s \hat{i}_i - e_{eq\_i} + k\,\mathrm{sgn}(i_i - \hat{i}_i) \\ \hat{e}_{i\_error} = -\dfrac{k}{\tau s + 1}\mathrm{sgn}(i_i - \hat{i}_i), \quad i \in (a,b,c) \\ \hat{e}_i = e_{eq\_i} + \hat{e}_{i\_error} \end{cases} \tag{8}$$

$$\begin{bmatrix} e_{eq\_a} \\ e_{eq\_b} \\ e_{eq\_c} \end{bmatrix} = \frac{L_m \omega_s}{L_r}\left[T_{dq/abc}\right]\begin{bmatrix} 0 & -1 \\ 1 & 0 \end{bmatrix}\begin{bmatrix} \psi_{rd} \\ \psi_{rq} \end{bmatrix} \tag{9}$$

where $\hat{\imath}_i$, $\hat{e}_{i\_error}$, and $\hat{e}_i$ are observed variables; *k* is the gain of the sliding mode observer, and $k > 0$; τ is time constant of the low-pass filter; $sgn()$ is the sign function. e_{eq_i} are the equivalent control terms in sliding mode control, $T_{dq/abc}$ is the inverse Park transformation, ψ_{rd} and ψ_{rq} are the rotor flux components in synchronous rotating reference frame. Other parameters definition and detailed derivation of equation (9) can be found in [35].

D. Residuals and Threshold

Based on the aforementioned robust differentiators and sliding mode observers, the estimated CCMVs can be expressed as follows:

$$\begin{cases} \hat{u}_{no\_a} = u_{ao}^* - R_s i_a - L_\sigma \dfrac{d\hat{i}_a}{dt} - \hat{e}_a \\ \hat{u}_{no\_b} = u_{bo}^* - R_s i_b - L_\sigma \dfrac{d\hat{i}_b}{dt} - \hat{e}_b \\ \hat{u}_{no\_c} = u_{co}^* - R_s i_c - L_\sigma \dfrac{d\hat{i}_c}{dt} - \hat{e}_c \end{cases} \tag{10}$$

where $\hat{u}_{no\_i}$ are the estimated values of CCMVs; $\frac{d\hat{i}_i}{dt}$ are the outputs of robust differentiators. $\hat{e}_i$ are the outputs of sliding mode observers, $i \in (a,b,c)$.

To identify the faults and fault switch positions, three residuals are defined:

$$\begin{cases} \varepsilon_{ab} = \hat{u}_{no\_a} - \hat{u}_{no\_b} \\ \varepsilon_{bc} = \hat{u}_{no\_b} - \hat{u}_{no\_c} \\ \varepsilon_{ca} = \hat{u}_{no\_c} - \hat{u}_{no\_a} \end{cases} \tag{11}$$

According to the equation (3) and (4) in Section II, three residuals are zero under normal operations. In the abnormal cases, assuming that T_1 suffers an open-switch fault, $i_a > 0$, and the obtained CCMVs are absolutely accurate, then u_{ao} is $-u_{dc}/2$. Equation (2) is rewritten as follows:

$$\begin{cases} u_{no\_a} = -\dfrac{u_{dc}}{2} - R_s i_a - L_\sigma \dfrac{di_a}{dt} - e_a \neq \hat{u}_{no\_a} \\ u_{no\_b} = u_{bo}^* - R_s i_b - L_\sigma \dfrac{di_b}{dt} - e_b = \hat{u}_{no\_b} \\ u_{no\_c} = u_{co}^* - R_s i_c - L_\sigma \dfrac{di_c}{dt} - e_c = \hat{u}_{no\_c} \end{cases} \tag{12}$$

where $u_{no\_a} = u_{no\_b} = u_{no\_c} = \hat{u}_{no\_b} = \hat{u}_{no\_c} \neq \hat{u}_{no\_a}$. According to (10), the equation (11) is revised as:

$$\begin{cases} \varepsilon_{ab} = \hat{u}_{no\_a} - u_{no\_a} = u_{ao}^* - u_{ao} = u_{ao}^* + \dfrac{u_{dc}}{2} \geq 0 \\ \varepsilon_{bc} = \hat{u}_{no\_b} - \hat{u}_{no\_c} = 0 \\ \varepsilon_{ca} = u_{no\_a} - \hat{u}_{no\_a} = -\varepsilon_{ab} = -u_{ao}^* - \dfrac{u_{dc}}{2} \leq 0 \end{cases} \tag{13}$$

Comparing the residuals between the normal and abnormal cases, an intuitive criteria of the open-switch fault is

$$\begin{cases} \varepsilon_{ab} > 0 \\ \varepsilon_{bc} = 0 \\ \varepsilon_{ca} < 0 \end{cases} \tag{14}$$

However, in practice, there are always some estimation errors in the CCMVs due to the effect of parameter variations and measurement noise. Thus, (14) cannot be used directly. The

This article has been accepted for publication in a future issue of this journal, but has not been fully edited. Content may change prior to final publication. Citation information: DOI 10.1109/TIE.2020.2965430, IEEE Transactions on Industrial Electronics

criteria of the fault identification shown in (14) is revised as:

$$\begin{cases} \varepsilon_{ab} \geq \varepsilon_0 \\ \left|\varepsilon_{bc}\right| \leq \varepsilon_0 \\ \varepsilon_{ca} \leq -\varepsilon_0 \end{cases} \tag{15}$$

where ε_0 is the threshold.

As well known, the threshold determines the robustness and sensitivity of a fault diagnosis algorithm. A small threshold implies high sensitivity but low robustness, and a large one means high robustness but low sensitivity. Thus, it is important to design a proper threshold.

Mathematically, the lower bound of the threshold must be greater than the largest absolute value of the three residuals in all possible normal operation conditions. And its upper bound must be less than the minimum absolute value of the three residuals in all possible abnormal operation conditions. However, it is not easy to calculate the lower and upper bound precisely due to the uncertainties in the system. Because there is another larger threshold which will be introduced in the next subsection in the proposed algorithm, the threshold ε_0 is selected by trial and error to make it slightly great than the largest absolute value of the three residuals in most normal operation conditions.

E. Active Common Mode Voltage Injection method

Based on the analysis above, the premise of the existence of a proper threshold is that the upper bound is greater than the lower one. And a long distance between the upper and lower bound of the threshold is the guarantee of the robustness and sensitivity of a fault diagnosis algorithm.

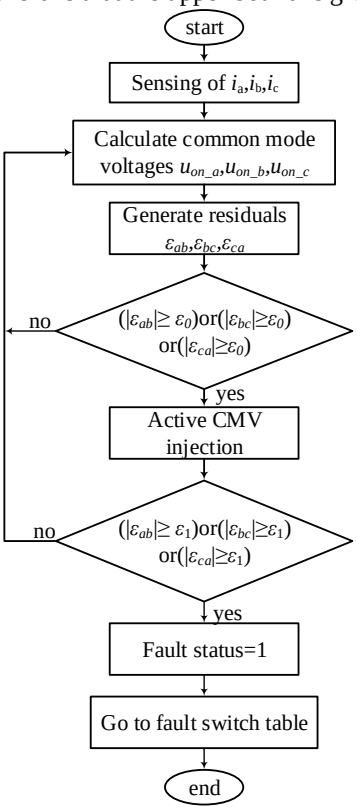

Fig. 3. The flowchart of the proposed fault-diagnosis algorithm.

To increase the distance, an active common mode voltage injection (ACMVI) method is introduced as follows:

According to (13), it can be found that ε_{ab} has a degree of freedom u_{no}^*, since $u_{ao}^* = u_{an}^* + u_{no}^*$ and u_{no}^* does not affect the output current in normal operation . We could actively use an optimal u_{no}^* to enlarge the difference between ε_{ab} and ε_0. The target to get the optimal u_{no}^* is equivalent to solving the optimization problem below:

$$\begin{cases} \max(\varepsilon_{ab}) \\ s.t.\ -\dfrac{u_{dc}}{2} - \min(u) \leq u_{no}^* \leq \dfrac{u_{dc}}{2} - \max(u) \end{cases} \tag{16}$$

where $u = [u_{an}^*, u_{bn}^*, u_{cn}^*]$. Note that the constraint of u_{no}^* mentioned in (15) is the precondition of linear modulation.

Because of the ACMVI, the resulting absolute value of the largest residuals in open-switch faults is increased. Thus, a larger threshold could be used to detect the fault as follows.

$$\begin{cases} \varepsilon_{ab} \geq \varepsilon_1 \\ \left|\varepsilon_{bc}\right| \leq \varepsilon_1 \\ \varepsilon_{ca} \leq -\varepsilon_1 \end{cases} \tag{17}$$

Because $\varepsilon_1 > \varepsilon_0$, the false alarms due to noises and parameter uncertainties will be reduced. The threshold ε_1 is selected to be slightly less than the minimum absolute value of the three residuals in all possible abnormal operation conditions.

TABLE II
RESIDUALS UNDER NORMAL AND FAULTY SITUATIONS

Single Open-switch Faults	Fault switch	Multiple Open-switch Faults	Fault switch
$\lvert\varepsilon_{ab}\rvert < \varepsilon_1$		①&&②	T_1,T_2
$\lvert\varepsilon_{bc}\rvert < \varepsilon_1$	–	①&&③	T_1,T_3
$\lvert\varepsilon_{ca}\rvert < \varepsilon_1$		①&&④	T_1,T_4
$\varepsilon_{ab} > \varepsilon_1$		①&&⑤	T_1,T_5
$\varepsilon_{ca} < -\varepsilon_1 \Rightarrow$ ①	T_1	①&&⑥	T_1,T_6
$\lvert\varepsilon_{bc}\rvert < \varepsilon_1$		②&&③	T_2,T_3
$\varepsilon_{ab} < -\varepsilon_1$		②&&④	T_2,T_4
$\varepsilon_{ca} > \varepsilon_1 \Rightarrow$ ②	T_2	②&&⑤	T_2,T_5
$\lvert\varepsilon_{bc}\rvert < \varepsilon_1$		②&&⑥	T_2,T_6
$\varepsilon_{bc} > \varepsilon_1$		③&&④	T_3,T_4
$\varepsilon_{ab} < -\varepsilon_1 \Rightarrow$ ③	T_3	③&&⑤	T_3,T_5
$\lvert\varepsilon_{ca}\rvert < \varepsilon_1$		③&&⑥	T_3,T_6
$\varepsilon_{bc} < -\varepsilon_1$		④&&⑤	T_4,T_5
$\varepsilon_{ab} > \varepsilon_1 \Rightarrow$ ④	T_4	④&&⑥	T_4,T_6
$\lvert\varepsilon_{ca}\rvert < \varepsilon_1$		⑤&&⑥	T_5,T_6
$\varepsilon_{ca} > \varepsilon_1$			
$\varepsilon_{bc} < -\varepsilon_1 \Rightarrow$ ⑤	T_5		
$\lvert\varepsilon_{ab}\rvert < \varepsilon_1$			
$\varepsilon_{ca} < -\varepsilon_1$			
$\varepsilon_{bc} > \varepsilon_1 \Rightarrow$ ⑥	T_6		
$\lvert\varepsilon_{ab}\rvert < \varepsilon_1$			

F. Overall Fault Diagnosis Algorithm

To reduce the rate of missed detection due to a too large threshold and false alarms due to a too small threshold, a fault diagnosis algorithm with double thresholds is introduced. The first small threshold ε_0 is used as the trigger condition for the ACMVI method. The second larger threshold ε_1 is used as the

This article has been accepted for publication in a future issue of this journal, but has not been fully edited. Content may change prior to final publication. Citation information: DOI 10.1109/TIE.2020.2965430, IEEE Transactions on Industrial Electronics

final decision condition for the faults. If an open-switch fault occurs, the residuals will exceed the first threshold and the ACMVI method will be triggered. It actively enlarges the residuals and make them quickly exceed the second threshold. As a result, the open-switch fault is detected. If the residuals exceed the first threshold due to measurement noise, parameter variations and other factors, the ACMVI method will not enlarge them and the false alarm can be avoided.

The overall fault-diagnosis flowchart is shown in Fig. 3. Table II is used to locate the fault switch positions. ①~⑥ represent the residuals conditions corresponding to six different single open-switch faults. If multiple open-switch faults happen, they could be identified from the combinations of ①~⑥.

TABLE III
PARAMETERS OF THE INDUCTION MOTOR SYSTEM

Parameters	Description	Value
P_n	Rated power	1.1kW
U_n	Rated voltage	220V
I_{rate}	Rated current	2.89A
n_{rate}	Rated speed	1390rpm
T_L	Rated torque	6Nm
R_s	Stator resistance	6.4Ω
R_r	Rotor resistance	4.8Ω
L_s	Stator self-inductance	0.364H
L_r	Rotor self-inductance	0.364H
L_m	Magnetizing inductance	0.336H
J	Moment of inertia	0.02kg.m^2
n_p	Number of pole pairs	2
V_{dc}	DC bus voltage	310V
α	Parameter of differentiator	2400
λ	Parameter of differentiator	1650
k	Gain of sliding mode observer	20
τ	Parameter of sliding mode observer	0.001
k_p	Proportional gain of current controller	16.8
k_i	Integral gain of current controller	3360

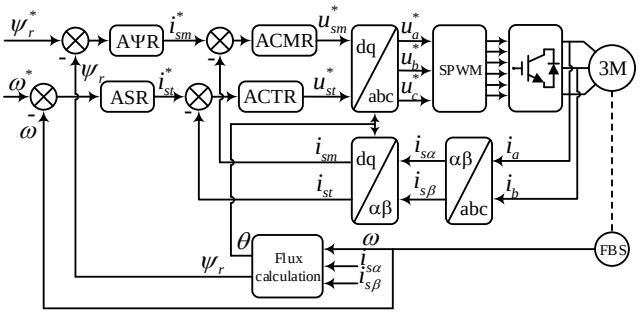

Fig. 4. The vector control of the VSI-Based IM system.

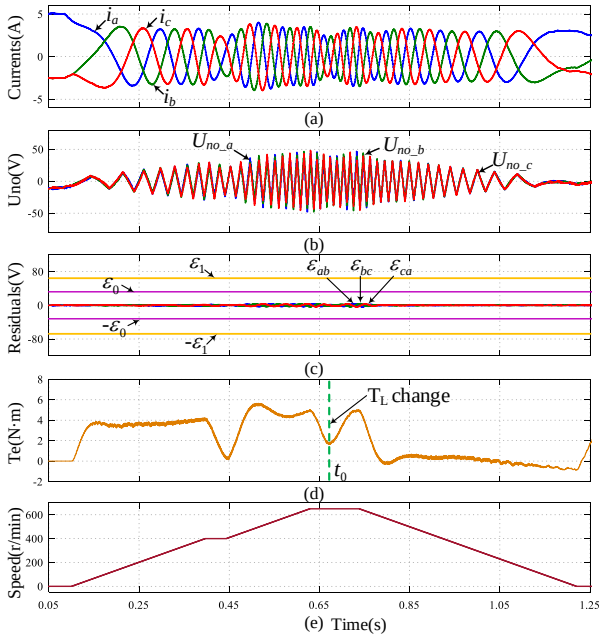

Fig. 5. Simulation results of VSI-IM system under the normal operation. (a) Measured three-phase load currents. (b) CCMVs. (c) Three residuals ε_{ab}, ε_{bc}, ε_{ca}. (d) The electromagnetic torque. (e) The speed of induction motor.

IV. SIMULATION RESULTS

In this section, a simulation built with MATLAB/Simulink is implemented to verify the effectiveness of the proposed diagnosis method. Parameters of the VSI-Based IM system are listed in Table III. And the vector control is adopted to control the IM [33], as shown in Fig. 4. In this system, the first threshold is selected to be 30V, and the second threshold is 60V. Their negative values are also used to detect the faults. To distinguish different fault switches, the fault flags are designed to be 0~6 corresponding to normal operation and T_1~T_6 open-switch fault operations respectively.

The simulation results in Fig. 5 show the state of the VSI-IM system under normal operating conditions. From the Fig. 5 (e), it can be seen that the IM speed accelerates from 0 r/min to 650 r/min. And the load of the IM suddenly increases to 3N·m at time t_0. During the whole process, three load currents of the motor are always sinusoidal. And the CCMVs of every phase U_{no_a} , U_{no_b} , U_{no_c} shown in Fig. 5 (b) are always approximately equal. As a result, three residuals ε_{ab}, ε_{bc}, ε_{ca} are all within the thresholds. These simulation results confirm that the proposed diagnosis method is insensitive to the system transients and changing load.

In Fig. 6, the effectiveness of the proposed ACMVI method is verified. When the open-switch fault first occurs at time t_1, the ACMVI method is not applied to the diagnosis algorithm. It is shown that the residuals are just over the first threshold ε_0 but below the second threshold ε_1. As a result, the open-switch fault detection is missed. At time t_2, the ACMVI method is applied and the residuals become much larger than before. The larger residuals exceed the second threshold ε_1 and the fault is detected. Therefore, this method can effectively reduce the rate of missed detection and improve the credibility of diagnostic results.

Fig. 7 shows simulation results under single open-switch fault operating conditions. At time t_3, the open-switch fault occurs on T_1. It can be seen that the load current of phase a drops to zero immediately, and the other currents are also affected. Then the calculated common mode voltage U_{no_a} is

This article has been accepted for publication in a future issue of this journal, but has not been fully edited. Content may change prior to final publication. Citation information: DOI 10.1109/TIE.2020.2965430, IEEE Transactions on Industrial Electronics

unequal to the other two voltages. As a result, the residuals ε_{ab}, ε_{ca} are out of the range of thresholds while the residual ε_{bc} is also nearly zero. Therefore, the fault switch T_1 can be located by the relationship of the residuals shown in Table II. At time t_4, we deliberately produce the residuals which are larger than ε_0 but less than ε_1, whereas there is no open-switch faults. It can be seen that the ACMVI method is triggered, but the resulting CCMVs are still equal to each other, which shows that the ACMVI method does not amplify the residuals in non-fault situations. Therefore, even if the residuals exceed the first threshold ε_0 due to some unexpected factors (open-switch faults are not included) in some harsh conditions, the ACMVI method could avoid false alarms successfully.

At time t_5 ,an open-switch fault occurs on T_2. The only difference between T_1 fault and T_2 fault is that the residuals ε_{ab}, ε_{ca} are opposite. At time t_6, an open-switch fault occurs on T_3. It can be seen that ε_{ab}, ε_{bc} exceed the second threshold ε_1, corresponding to the fault on T_3. If other single open-switch faults happen, similar analysis could be conducted.

Fig. 8 shows simulation results under multiple open-switch faults operating conditions. At time t_7, a multiple open-switch fault occurs on T_1 and T_5. It can be seen that the residuals have two conditions ① and ⑤ in Table II. At time t_8, an open-phase fault occurs on phase a, and the conditions ① ② are also shown in Fig. 8 (c). At time t_9, a multiple open-switch fault occurs on T_3 and T_6, corresponding to the conditions ③ and ⑥. If other multiple open-switch faults occur, all residuals conditions correspond to the states shown in Table II. Finally, the above simulation results validate the effectiveness and high robustness of the proposed fault diagnosis method.

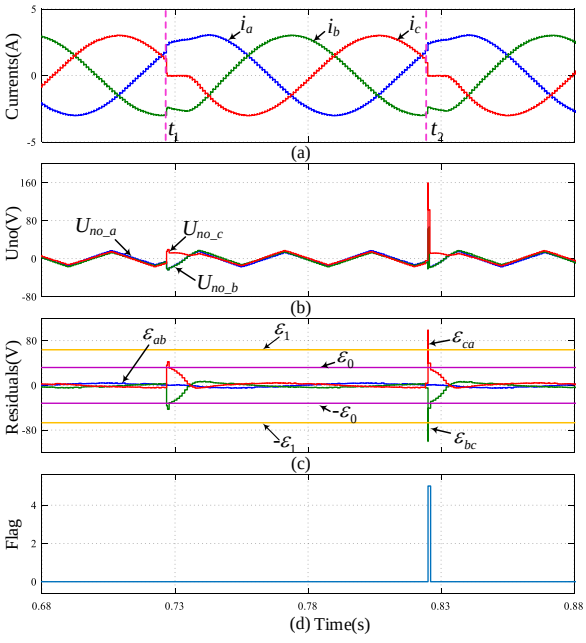

Fig. 6. Comparison results between ACMVI method and non-ACMVI method (a) Measured three-phase load currents. (b) CCMVs. (c) Three residuals ε_{ab}, ε_{bc}, ε_{ca}. (d) The fault flag.

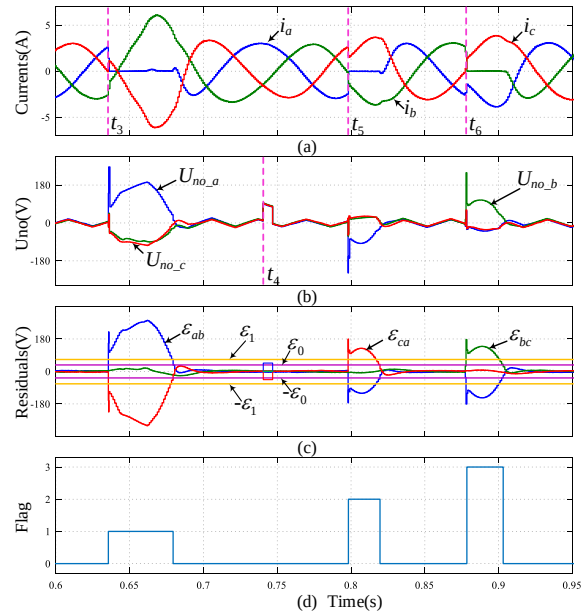

Fig. 7. Simulation results of VSI-IM system under single open-switch fault operations. (a) Measured three-phase load currents. (b) CCMVs. (c) Three residuals ε_{ab}, ε_{bc}, ε_{ca}. (d) The fault flag.

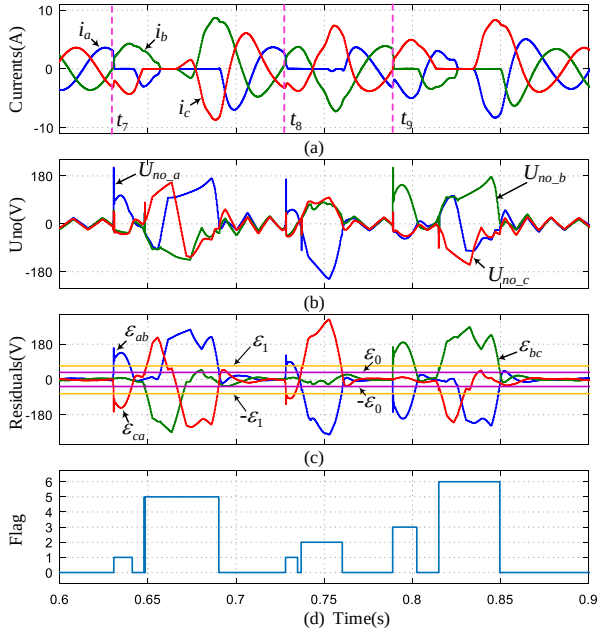

Fig. 8. Simulation results of VSI-IM system under multiple open-switch fault operations. (a) Measured three-phase load currents. (b) CCMVs. (c) Three residuals ε_{ab}, ε_{bc}, ε_{ca}. (d) The fault flag.

V. Experimental Results

In this section, the proposed open-switch fault diagnosis method is further investigated in an experimental prototype. As shown in Fig. 9, a dSpace-DS1202 board is used to control the VSI, and a PC is used to communicate with the dSpace by an ethernet cable. There is an extended interface board between the dSpace and inverter, which is used to achieve signal acquisition and signal processing. A conventional diode-uncontrolled rectifier is used to generate the DC voltage which is 310V. The motor1 is an IM driven by the inverter. The motor2 is a PMSM used as the load. The parameters of the system are shown in

This article has been accepted for publication in a future issue of this journal, but has not been fully edited. Content may change prior to final publication. Citation information: DOI 10.1109/TIE.2020.2965430, IEEE Transactions on Industrial Electronics

Table III. The sampling period of the system is 50us, and the switching frequency of the VSI is 10 kHz. The one-step Euler method is used in the discrete time realization of the differentiator and sliding mode observers [34] with a sampling period of 50us. In experiments, the current information obtained by an interface board and the other related variables in the controller are transmitted to the PC through the ethernet cable. And they could be conveniently displayed and stored in the ControDesk (software for dSpace-DS1202). Moreover, all the data could be saved as CSV files and imported into Matlab for redrawing. And the following figures in experimental parts are obtained in this way.

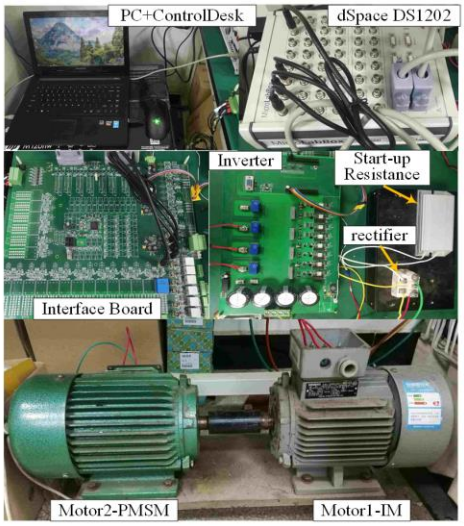

Fig. 9. Photograph of the dSpace-Based experimental platform.

A. Effect of Parameter Variations

Due to the parameter variations and measurement noises, the residuals will fluctuate around zero even under normal conditions. The effect of parameter variations on residuals is shown in Fig. 10. At time t_1, 20% parameter deviations relative to nominal parameters (stator resistance R_s, stator inductance L_s) of the real plant are imposed, and the magnitude of the residuals increase to about 15V. At time t_2, 40% parameter deviations are applied to the model. The resulting residuals increase to nearly 26V. Taking into account the robustness and sensitivity of fault diagnosis, the first threshold is selected to be 30V. To ensure high robustness and reliability, and the second large threshold is 60V in this experiment.

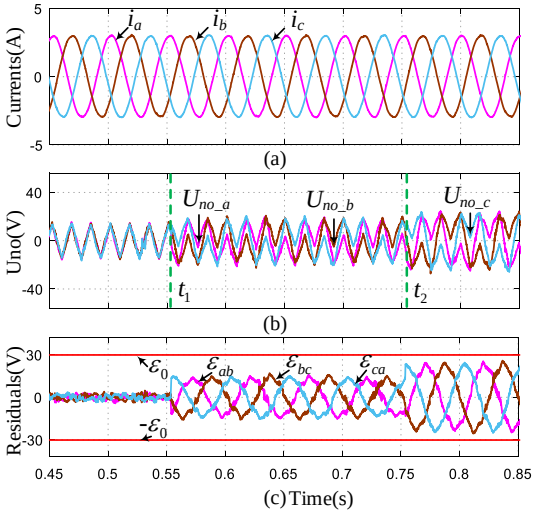

Fig. 10. Experimental results of the effect of parameter variations. (a) Measured three-phase load currents. (b) CCMVs. (c) Three residuals ε_{ab}, ε_{bc}, ε_{ca}.

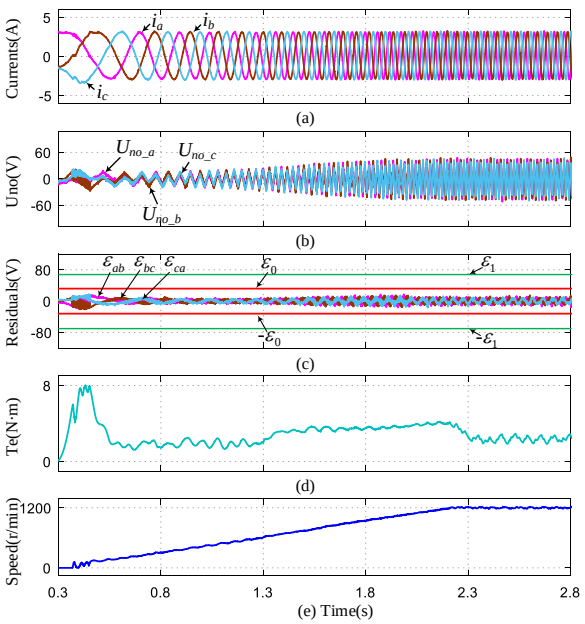

Fig. 11. Experimental results of IM system from 0 to 1200r/min, 30% load (a) Measured three-phase load currents. (b) CCMVs. (c) Three residuals ε_{ab}, ε_{bc}, ε_{ca}. (d) The electromagnetic torque. (e) The speed of induction motor.

B. Transients and Load Variations

Fig. 11 and 12 show the experimental results of the VSI-IM system under the transients and load variations. And due to the limitation of DC voltage, Flux-weakening control is used at high speeds. In Fig. 11, the IM start from 0r/min and accelerates to 1200r/min, and 30% load is applied to it at 1.3s. During this process, it can be seen that three CCMVs shown in Fig. 11 (b) are always nearly equal and three residuals ε_{ab}, ε_{bc}, ε_{ca} are all within the thresholds. Fig. 12 shows the results when the IM load is suddenly changed from no load to the rated load at 1200r/min. As shown in the Fig. 12 (b), the residuals become larger than before and the peak value appears during the transients, but they are still within the first threshold ε_0. Clearly, they will also not exceed the second threshold ε_1, avoiding false alarms. These experimental results can validate that the thresholds can effectively guarantee the robustness of the diagnosis system during the transients and load variations.

C. ACMVI Method and Single Switch Faults

Since the second threshold is relatively large, the residuals may be only larger than the first threshold ε_0 but less than the second one ε_1 in some fault conditions, resulting in missed detection and low sensitivity. To overcome this problem, the ACMVI method is applied.

Fig. 13 and Fig. 14 show the comparative results between the ACMVI method and non-ACMVI method. In these experiments, the motor runs at 300r/min with 20% load.

This article has been accepted for publication in a future issue of this journal, but has not been fully edited. Content may change prior to final publication. Citation information: DOI 10.1109/TIE.2020.2965430, IEEE Transactions on Industrial Electronics

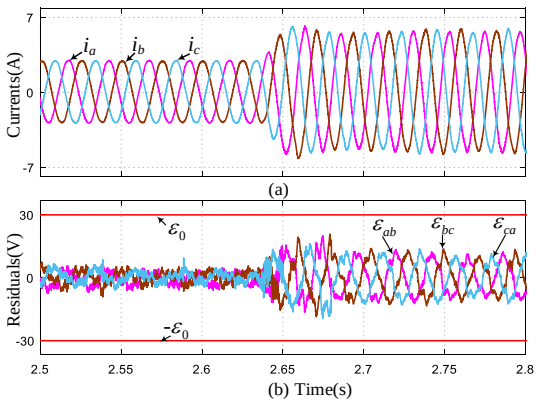

Fig. 12. Experimental results of IM system from no load to rated load at 1200r/min. (a) Measured three-phase load currents. (b) Three residuals ε_{ab}, ε_{bc}, ε_{ca}.

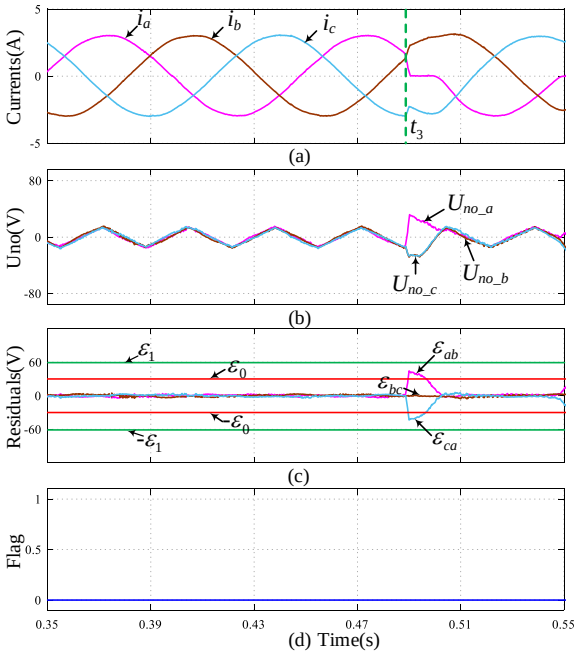

Fig. 13. Experimental results without the ACMVI method, 300r/min, 20% load. (a) Measured three-phase load currents. (b) CCMVs. (c) Three residuals ε_{ab}, ε_{bc}, ε_{ca}. (d) The fault flag.

In Fig. 13, an open-switch fault occurs on the IGBT T_1 at time t_3, and the ACMVI method is not applied to the diagnosis algorithm. It is shown that the residuals are just over the first threshold ε_0 but below the second threshold ε_1. As a result, the open-switch fault detection is missed. In Fig. 14, an open-switch fault occurs on the IGBT T_1 at the same current angle. The ACMVI method is applied and the residuals become much larger than before. The larger residuals exceed the second threshold ε_1 and the fault is detected. From these results, it can be seen that this method can effectively increase the values of the residuals after the fault occurs, which could reduce the rate of missed detection.

In Fig. 15, an open-switch fault still occurs on the IGBT T_1 at time t_4, when the IM runs at 1200r/min with 80% load. And it also shows the performance of the back EMFs observer and robust differentiator. As we can see, the output of the observer and differentiator is very smooth and sinusoidal.

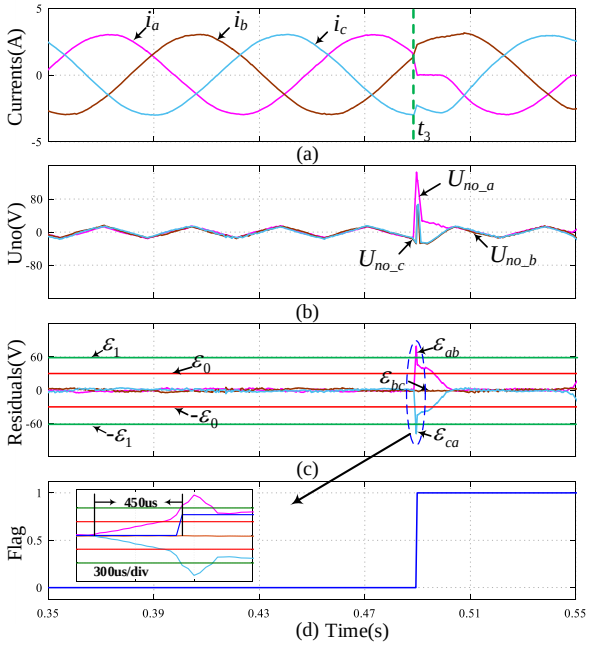

Fig. 14. Experimental results with the ACMVI method,300r/min,20% load. (a) Measured three-phase load currents. (b) CCMVs. (c) Three residuals ε_{ab}, ε_{bc}, ε_{ca}. (d) The fault flag.

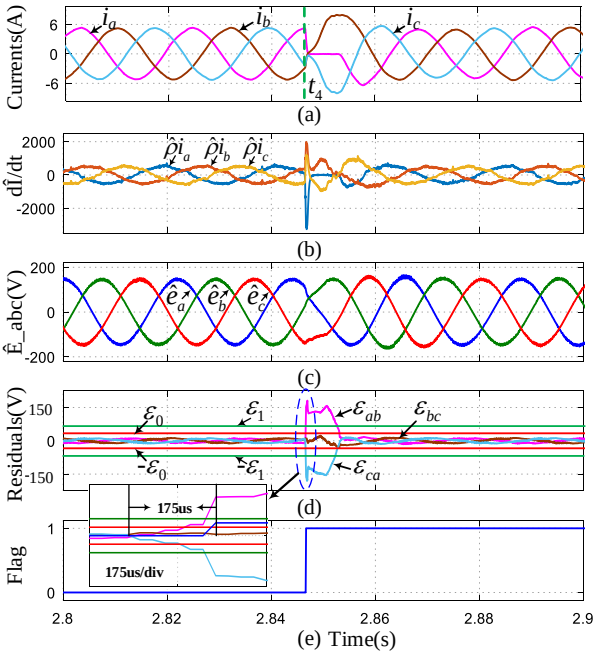

Fig. 15. Experimental results of IM system under the T_1 fault operation, 1200r/min, 80% load. (a) Measured three-phase load currents. (b) The estimations of currents derivative. (c) The estimations of back EMFs. (d) Three residuals ε_{ab}, ε_{bc}, ε_{ca}. (e) The fault flag.

Fig. 16 show experimental results under the effect of noises and the T_3 open-switch fault. At time t_5, we deliberately add disturbances to the system. As a result, the residuals are larger than ε_0 but less than ε_1, and the ACMVI method is triggered. As can be seen from the enlarged part in Fig. 16 (b) and (c), the residuals still retain their original value, which shows that the ACMVI method does not amplify the residuals in non-fault situations. Therefore, even if the residuals exceed the first threshold ε_0 due to some unexpected factors in some harsh con-

This article has been accepted for publication in a future issue of this journal, but has not been fully edited. Content may change prior to final publication. Citation information: DOI 10.1109/TIE.2020.2965430, IEEE Transactions on Industrial Electronics

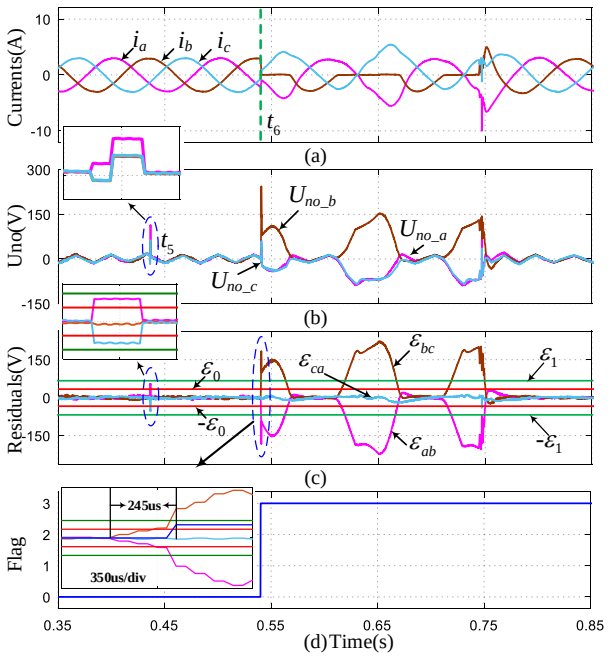

Fig. 16. Experimental results of IM system under the T_3 fault operation, 300r/min, 20% load. (a) Measured three-phase load currents. (b) CCMVs. (c) Three residuals ε_{ab}, ε_{bc}, ε_{ca}. (d) The fault flag.

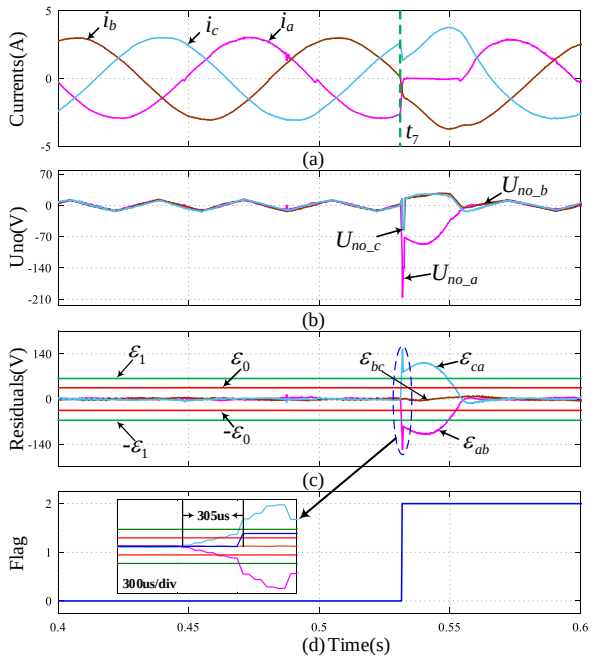

Fig. 17. Experimental results of IM system under the T_2 fault operation, 300r/min, 20% load.(a) Measured three-phase load currents. (b) CCMVs. (c) Three residuals ε_{ab}, ε_{bc}, ε_{ca}. (d) The fault flag.

ditions, the ACMVI method could avoid false alarms successfully. At time t_6, an open-switch fault occurs on the IGBT T_3. As a result, the residuals ε_{ab}, ε_{bc} exceed the range of threshold value at once, while ε_{ca} is still under the threshold.

In Fig. 17, an open-switch fault occurs on the IGBT T_2 at time t_7, the performance of the residuals is completely opposite to that when open-switch fault occurs on T_1. As for other single open-switch faults, they can all be detected and located by looking up the Table II.

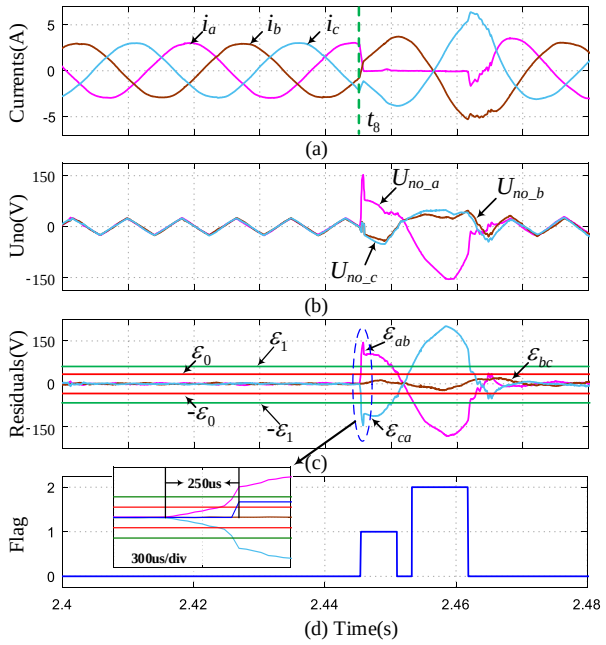

Fig. 18. Experimental results of IM system under the T_1 and T_2 faults operation, 1200r/min, 20% load.(a) Measured three-phase load currents. (b) CCMVs. (c) Three residuals ε_{ab}, ε_{bc}, ε_{ca}. (d) The fault flag.

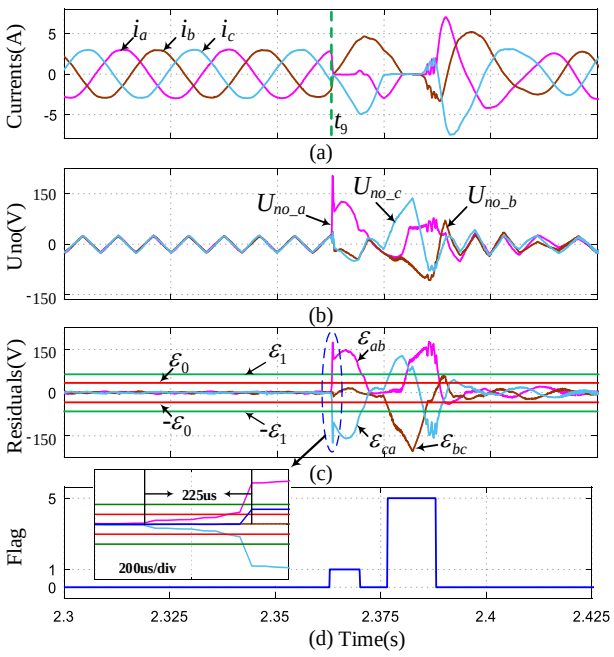

Fig. 19. Experimental results of IM system under the T_1 and T_5 faults operation, 1200r/min, 20% load.(a) Measured three-phase load currents. (b) CCMVs. (c) Three residuals ε_{ab}, ε_{bc}, ε_{ca}. (d) The fault flag.

D. Multiple Switch Faults and Small Current Situation

The experiment results of open-phase faults and multiple open-switch faults are shown in Fig. 18 and Fig. 19. In Fig. 18, the "OFF" signals are imposed on the IGBT T_1 and T_2 at the same time, and the open-switch fault on T_1 is firstly detected and located. After a while, the fault on T_2 is also detected. In Fig. 19, the multiple open-switch faults occur on the IGBT T_1 and T_5 at time t_9, corresponding to the conditions ① and ⑤ in

This article has been accepted for publication in a future issue of this journal, but has not been fully edited. Content may change prior to final publication. Citation information: DOI 10.1109/TIE.2020.2965430, IEEE Transactions on Industrial Electronics

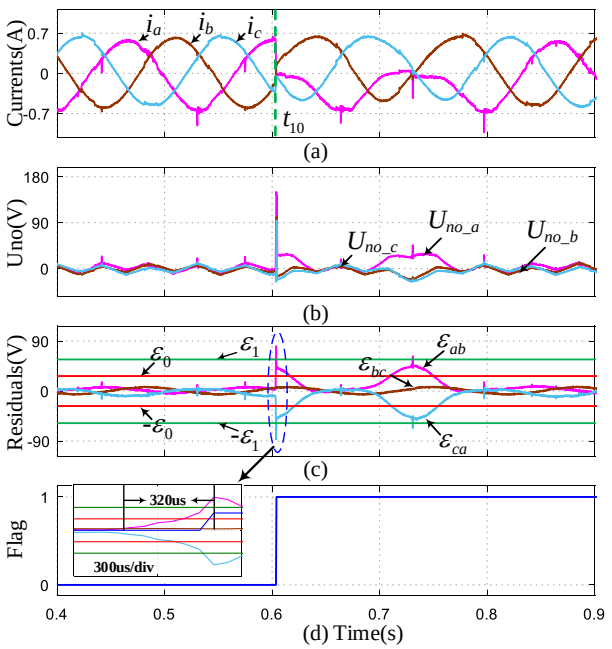

Fig. 20. Experimental results under the small currents situation. (a) Measured three-phase load currents. (b) CCMVs. (c) Three residuals ε_{ab}, ε_{bc}, ε_{ca}. (d) The fault flag.

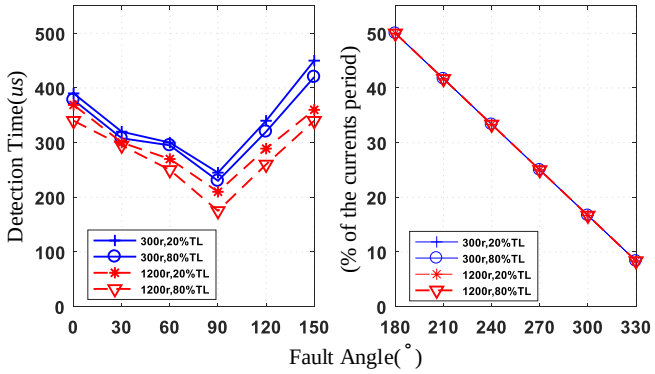

Fig. 21. The detection times of an open-switch fault in the IGBT T_1 under different system conditions.

the Table II. If other multiple open-switch faults occur, all residuals conditions correspond to the states shown in Table II.

In Fig. 20, the robustness and effectiveness of the proposed diagnostic method under the small currents condition are demonstrated. To construct such an operation condition, we change a low current induction motor.

As can be seen from the Fig. 20 (c), due to the effect of measurement noise and uncertainties, the residuals are close to the first threshold ε_0 under non-fault situations, but the diagnosis algorithm is still robust due to the existence of the second threshold ε_1. At time t_{10}, an open-switch fault occurs on T_1. The fault is detected and located quickly and accurately, which demonstrates the effectiveness of the method under this situation.

E. Detection Time

Fig. 21 shows the detection times of an open-switch fault in the IGBT T_1 under different conditions. As seen, if an open-switch fault occurs on T_1 when $i_a > 0$, the fault can be quickly detected, and the average detection time is about 300us. If an open-switch fault occurs on T_1 when $i_a < 0$, the fault does not affect the output currents until $i_a = 0$. Thus, in the worst cases, the open-switch fault is undetectable for half a period of the output currents.

VI. Conclusion

A fast and reliable method for diagnosis open-switch faults in VSI-Based IM systems is proposed in this paper. This approach is based on the common mode voltages calculated from the switching average model of the IM system. Three CCMVs are supposed to be equal to each other under the normal operating condition, while they become unequal if an open-switch fault occurs. This feature is used to detect and locate the fault switches of the inverter. The proposed fault-diagnosis algorithm only requires the measured current information, avoiding the use of additional sensors. And considering the effect of parameter variations and measurement noises, two thresholds are used to reduce the rate of false alarms, improving the robustness of the diagnostic system. In addition, an active common mode voltage injection (ACMVI) method is proposed to improve the reliability and sensitivity of the diagnosis system. It takes advantage of a degree of freedom in the modulation so that the fault information can be highlighted when an open-switch fault occurs, increasing the credibility of the diagnosis system.

The application of these methods can simultaneously ensure the system's high immunity to false alarms and high sensitivity to open-switch faults. Experimental and simulated results have validated the effectiveness and high robustness of the proposed fault-diagnosis technique, which can be easily embedded into the ac drive software without extra cost.

References

[1] D. U. Campos-Delgado, D. R. Espinoza-Trejo and E. Palacios, "Fault-tolerant control in variable speed drives: a survey," in *IET Electric Power Applications*, vol. 2, no. 2, pp. 121-134, March 2008.

[2] L. Li, Y. Sun, H. Han, G. Shi, M. Su and M. Zheng, "A Decentralized Control for Cascaded Inverters in Grid-connected Applications," in *IEEE Transactions on Industrial Electronics*, early access, 2019.https://doi.org/10.1109/TIE.2019.2945266.

[3] X. Hou, Y. Sun, X. Zhang, J. Lu, P. Wang and J. M. Guerrero, "Improvement of Frequency Regulation in VSG-Based AC Microgrid via Adaptive Virtual Inertia," in *IEEE Transactions on Power Electronics*. doi: 10.1109/TPEL.2019.2923734

[4] Y. Song and B. Wang, "Survey on Reliability of Power Electronic Systems," in *IEEE Transactions on Power Electronics*, vol. 28, no. 1, pp. 591-604, Jan. 2013.

[5] B. Tabbache, M. Benbouzid, A. Kheloui, J. M. Bourgeot, and A. Mamoune, "An improved fault-tolerant control scheme for PWM inverter-fed induction motor-based EVs," *ISA Trans.*, vol. 52, no. 6, pp. 862–869, 2013.

[6] B. Lu and S. K. Sharma, "A Literature Review of IGBT Fault Diagnostic and Protection Methods for Power Inverters," in *IEEE Transactions on Industry Applications*, vol. 45, no. 5, pp. 1770-1777, Sept.-oct. 2009.

[7] K. Rothenhagen and F. W. Fuchs, "Performance of diagnosis methods for IGBT open circuit faults in three phase voltage source inverters for AC variable speed drives," *2005 European Conference on Power Electronics and Applications*, Dresden, 2005, pp. 10 pp.-P.7.

[8] A. M. S. Mendes, A. J. M. Cardoso and E. S. Saraiva, "Voltage source inverter fault diagnosis in variable speed AC drives, by Park's vector approach," *1998 Seventh International Conference on Power Electronics and Variable Speed Drives (IEE Conf. Publ. No. 456)*, London, UK, 1998, pp. 538-543.

[9] D. Diallo, M. E. H. Benbouzid, D. Hamad and X. Pierre, "Fault detection and diagnosis in an induction Machine drive: a pattern recognition approach based on concordia stator mean current vector," in *IEEE Transactions on Energy Conversion*, vol. 20, no. 3, pp. 512-519, Sept. 2005.

[10] J. O. Estima and A. J. Marques Cardoso, "A New Approach for Real-Time Multiple Open-Circuit Fault Diagnosis in Voltage-Source Inverters," in *IEEE Transactions on Industry Applications*, vol. 47, no. 6, pp. 2487-2494, Nov.-Dec. 2011.

[11] Z. Jian-Jian, C. Yong, C. Zhang-Yong and Z. Anjian, "Open-Switch Fault Diagnosis Method in Voltage-Source Inverters Based on Phase Currents," in *IEEE Access*, vol. 7, pp. 63619-63625, 2019.

[12] H. Zhao and L. Cheng, "Open-Switch Fault-Diagnostic Method for Back-to-Back Converters of a Doubly Fed Wind Power Generation System," in *IEEE Transactions on Power Electronics*, vol. 33, no. 4, pp. 3452-3461, April 2018.

[13] R. Peuget, S. Courtine and J. Rognon, "Fault detection and isolation on a PWM inverter by knowledge-based model" in *IEEE Transactions on Industry Applications*, vol. 34, no. 6, pp. 1318-1326, Nov.-Dec. 1998.

[14] M. Trabelsi, M. Boussak and M. Gossa, "Multiple IGBTs open circuit faults diagnosis in voltage source inverter fed induction motor using modified slope method," *The XIX International Conference on Electrical Machines* - ICEM 2010, Rome, 2010, pp. 1-6.

[15] Q. An, L. Sun and L. Sun, "Current Residual Vector-Based Open-Switch Fault Diagnosis of Inverters in PMSM Drive Systems," in *IEEE Transactions on Power Electronics*, vol. 30, no. 5, pp. 2814-2827, May 2015.

[16] H. T. Eickhoff, R. Seebacher, A. Muetze and E. G. Strangas, "Enhanced and Fast Detection of Open-Switch Faults in Inverters for Electric Drives," in *IEEE Transactions on Industry Applications*, vol. 53, no. 6, pp. 5415-5425, Nov.-Dec. 2017.

[17] I. Jlassi, J. O. Estima, S. K. El Khil, N. M. Bellaaj and A. J. M. Cardoso, "A Robust Observer-Based Method for IGBTs and Current Sensors Fault Diagnosis in Voltage-Source Inverters of PMSM Drives," in *IEEE Transactions on Industry Applications*, vol. 53, no. 3, pp. 2894-2905, May-June 2017.

[18] I. P. Georgakopoulos, E. D. Mitronikas and A. N. Safacas, "Detection of Induction Motor Faults in Inverter Drives Using Inverter Input Current Analysis," in *IEEE Transactions on Industrial Electronics*, vol. 58, no. 9, pp. 4365-4373, Sept. 2011.

[19] R. L. de Araujo Ribeiro, C. B. Jacobina, E. R. C. da Silva and A. M. N. Lima, "Fault detection of open-switch damage in voltage-fed PWM motor drive systems," in *IEEE Transactions on Power Electronics*, vol. 18, no. 2, pp. 587-593, March 2003.

[20] M. Trabelsi, M. Boussak, and M. Gossa, "PWM-Switching pattern-based diagnosis scheme for single and multiple open-switch damages in VSI-fed induction motor drives," *ISA Trans.*, vol. 51, no. 2, pp. 333–344, 2012.

[21] J. Hang, J. Zhang, M. Cheng and S. Ding, "Detection and Discrimination of Open-Phase Fault in Permanent Magnet Synchronous Motor Drive System," in *IEEE Transactions on Power Electronics*, vol. 31, no. 7, pp. 4697-4709, July 2016.

[22] S. Karimi, P. Poure and S. Saadate, "Fast power switch failure detection for fault tolerant voltage source inverters using FPGA," in *IET Power Electronics*, vol. 2, no. 4, pp. 346-354, July 2009.

[23] S. Karimi, A. Gaillard, P. Poure and S. Saadate, "FPGA-Based Real-Time Power Converter Failure Diagnosis for Wind Energy Conversion Systems," in *IEEE Transactions on Industrial Electronics*, vol. 55, no. 12, pp. 4299-4308, Dec. 2008.

[24] M. A. Rodriguez-Blanco *et al*., "A Failure-Detection Strategy for IGBT Based on Gate-Voltage Behavior Applied to a Motor Drive System," in *IEEE Transactions on Industrial Electronics*, vol. 58, no. 5, pp. 1625-1633, May 2011.

[25] C. Shu, C. Ya-Ting, Y. Tian-Jian and W. Xun, "A Novel Diagnostic Technique for Open-Circuited Faults of Inverters Based on Output Line-to-Line Voltage Model," in *IEEE Transactions on Industrial Electronics*, vol. 63, no. 7, pp. 4412-4421, July 2016.

[26] Z. Huang, Z. Wang and H. Zhang, "A Diagnosis Algorithm for Multiple Open-Circuited Faults of Microgrid Inverters Based on Main Fault Component Analysis," in *IEEE Transactions on Energy Conversion*, vol. 33, no. 3, pp. 925-937, Sept. 2018.

[27] H. Dan *et al*., "Error-Voltage-Based Open-Switch Fault Diagnosis Strategy for Matrix Converters with Model Predictive Control Method," in *IEEE Transactions on Industry Applications*, vol. 53, no. 5, pp. 4603-4612, Sept.-Oct. 2017.

[28] D. Zhou, S. Yang and Y. Tang, "A Voltage-Based Open-Circuit Fault Detection and Isolation Approach for Modular Multilevel Converters With Model-Predictive Control," in *IEEE Transactions on Power Electronics*, vol. 33, no. 11, pp. 9866-9874, Nov. 2018.

[29] I. González-Prieto, M. J. Duran, N. Rios-Garcia, F. Barrero and C. Martín, "Open-Switch Fault Detection in Five-Phase Induction Motor Drives Using Model Predictive Control," in *IEEE Transactions on Industrial Electronics*, vol. 65, no. 4, pp. 3045-3055, April 2018.

[30] N. M. A. Freire, J. O. Estima and A. J. M. Cardoso, "A Voltage-Based Approach Without Extra Hardware for Open-Circuit Fault Diagnosis in Closed-Loop PWM AC Regenerative Drives," in *IEEE Transactions on Industrial Electronics*, vol. 61, no. 9, pp. 4960-4970, Sept. 2014.

[31] S. Khomfoi and L. M. Tolbert, "Fault Diagnosis and Reconfiguration for Multilevel Inverter Drive Using AI-Based Techniques," in *IEEE Transactions on Industrial Electronics*, vol. 54, no. 6, pp. 2954-2968, Dec. 2007.

[32] Levant. A, "Robust exact differentiation via sliding mode technique," *Automatica*, 34(3):379-384, 1998.

[33] Peter Vas. *Vector Control of AC Machines*. New York: Oxford University Press, 1990.

[34] Livne M, Levant A. "Proper discretization of homogeneous differentiators ". *Automatica*, 2014, 50(8):2007-2014.

[35] Bensiali, N. , E. Etien , and N. Benalia . "Convergence analysis of back-EMF MRAS observers used in sensorless control of induction motor drives." *Mathematics and Computers in Simulation* 115(2015).

Yitao Cheng was born in Hebei, China, in 1995. He received the B.S. degree in electronic engineering from Central South University, Changsha, China, in 2017, where he is currently working toward the M.S. degree in electrical engineering.

His research interests include motor drives and fault diagnosis.

Yao Sun (M'13) was born in Hunan, China, in 1981. He received the B.S., M.S. and Ph.D. degrees from Central South University, Changsha, China, in 2004, 2007 and 2010, respectively. He has been a Professor with the School of Automation, Central South University, China.

His research interests include matrix converter, micro-grid and wind energy conversion system

Xing Li was born in Hunan, China, in 1988. She received the B.S. and Ph.D. degrees from Central South University, Changsha, China, in 2009 and 2014, respectively. She is currently an Associate Professor with the College of Electrical and Information Engineering, Hunan University, Changsha, China.

Her research interests include power electronic converter and wind energy conversion system.

This article has been accepted for publication in a future issue of this journal, but has not been fully edited. Content may change prior to final publication. Citation information: DOI 10.1109/TIE.2020.2965430, IEEE Transactions on Industrial Electronics

Hanbing Dan was born in Hubei, China, in 1991. He received the B.S. degree in Automation, and Ph.D. degree in Control Science and Engineering from Central South University, Changsha, China, in 2012, and 2017, respectively. He was a visiting researcher in Faculty of Engineering at the University of Nottingham, United Kingdom during 2017. He is currently an associate professor with the School of Automation, Central South University, China.

His research interests include power converter, motor control, model predictive control, fault diagnosis.

Jianheng Lin was born in Fujian, China, in 1994. He received the B.S. degree in electronic engineering from Jimei University, Xiamen, China, in 2016. He is currently working toward the Ph.D. degree in control science and engineering at the Central South University, Changsha.

His research interests include linear time periodic system analysis and matrix converters.

Mei Su was born in Hunan, China, in 1967. She received the B.S., M.S. and Ph.D. degrees from the School of Information Science and Engineering, Central South University, Changsha, China, in 1989, 1992 and 2005, respectively. She has been a Full Professor with the School of Automation, Central South University. She is currently an Associate Editor of the IEEE Transactions on Power Electronics.

Her research interests include matrix converter, adjustable speed drives, and wind energy conversion system.